NIH Public Access
Author Manuscript
Osteoarthritis Cartilage. Author manuscript; available in PMC 2014 January 01.

Published in final edited form as:
Osteoarthritis Cartilage. 2013 January ; 21(1): 94–101. doi:10.1016/j.joca.2012.09.008.

Bone and Cartilage Demonstrate Changes Localized to Bone Marrow Edema-like Lesions within Osteoarthritic Knees

Galateia J Kazakia[1], **Daniel Kuo**[1], **Joseph Schooler**[1], **Sarmad Siddiqui**[1], **Swetha Shanbhag**[2], **Gregory Bernstein**[2], **Andrew Horvai**[3], **Sharmila Majumdar**[1,2], **Michael Ries**[4], and **Xiaojuan Li**[1]

[1]Musculoskeletal Quantitative Imaging Research Group, Department of Radiology and Biomedical Imaging, University of California, San Francisco; San Francisco, CA USA

[2]University of California, Berkeley; Berkeley, CA USA

[3]Department of Pathology, University of California, San Francisco; San Francisco, CA USA

[4]Department of Orthopaedic Surgery, University of California, San Francisco; San Francisco, CA USA

Abstract

Objective—Our objective is to understand the biological and mechanical pathways linking cartilage, bone, and marrow changes in the progression of osteoarthritis (OA). The aim of the present study was to evaluate bone structure and composition within bone marrow edema-like lesion (BMEL) regions associated with knee OA.

Methods—Tibial plateau specimens (n = 18) were collected from 10 subjects with knee OA scheduled for total knee arthroplasty (TKA). Magnetic resonance (MR) imaging was used to identify BMEL and quantify metrics of cartilage composition. Micro-computed tomography (μCT) and high-resolution peripheral quantitative computed tomography (HR-pQCT) were used to quantify density and microstructure of the subchondral trabecular bone. Fourier transform infrared (FTIR) spectroscopy was used to quantify tissue composition.

Corresponding author: Galateia J. Kazakia, Musculoskeletal Quantitative Imaging Research Group, Department of Radiology and Biomedical Imaging, University of California, San Francisco, 185 Berry St, Suite 350, San Francisco, CA 94107, Tel: +1 (415) 353-4534, Fax: +1 (415) 353-9423, galateia.kazakia@ucsf.edu.
Galateia J. Kazakia galateia.kazakia@ucsf.edu
Daniel Kuo dankuo@gmail.com
Joseph Schooler joseph.schooler@ucsf.edu
Sarmad Siddiqui sarmadsiddiqui@gmail.com
Swetha Shanbhag swshanbh@ucsd.edu
Gregory Bernstein gregb@berkeley.edu
Andrew Horvai Andrew.Horvai@ucsf.edu
Sharmila Majumdar sharmila.majumdar@radiology.ucsf.edu
Michael Ries riesm@orthosurg.ucsf.edu
Xiaojuan Li Xiaojuan.li@ucsf.edu

Author Contributions
All authors have made substantial contributions to study execution, manuscript preparation, and final approval of the submitted article. GJK (galateia.kazakia@ucsf.edu) and XL (xiaojuan.li@ucsf.edu) take responsibility for the integrity of the work as a whole.

Conflict of Interest
None

Results—Trabecular bone within BMEL was higher in volume fraction, with more and thicker trabeculae that were more plate-like in structure compared to unaffected regions. BMEL trabecular tissue composition had decreased phosphate and carbonate content. Marrow infiltration by a fibrous collagen network and evidence of increased bone remodeling were present. Structural and compositional changes were specifically localized to regions underlying cartilage degradation.

Conclusion—These results support the paradigm of focal interactions among bone, marrow, and cartilage in the progression of knee OA. Quantitative evaluation of tissue changes and interactions may aid in the understanding of disease pathophysiology and provide imaging markers for disease progression.

Keywords

osteoarthritis; knee; marrow lesion; edema; subchondral bone; histopathology; CT; MRI; FTIR; tissue quality

Introduction

Osteoarthritis (OA) is a disease in which multiple components interact and lead collectively to joint failure. In OA, cartilage pathology is accompanied by alterations within subchondral bone and marrow space. While it is clear that the entire joint is involved in OA etiopathogenesis, neither the initiation, sequence nor causative relationships between changes in bone, marrow, and cartilage compartments are understood. Improved understanding of the OA joint environment could accelerate development of prognostic markers for the disease and identification of early therapeutic targets.

Through the use of magnetic resonance imaging (MRI), a relationship has been reported between the presence of osteoarthritic cartilage degradation and bone marrow edema-like lesions (BMEL) in the subchondral trabecular bone compartment, identified as regions of hyperintense signal on T2-weighted fat saturated MR images [1]. Existence of BMEL has been associated with OA pain [2,3] and progression of clinical manifestations of OA [4,5]. Further, focal cartilage lesions have been shown to be preferentially located in proximity to regions of BMEL [6]. MRI $T_{1\rho}$ value, an indicator of early cartilage degradation, is elevated in cartilage overlying BMEL in OA [6] and in patients with recent knee trauma [7], with the level of cartilage degradation proportional to BMEL signal intensity. Additionally, cartilage overlying BMEL shows greater increase over time in degradation markers than surrounding cartilage [6]. Therefore BMEL regions appear to be consistently and fundamentally involved in OA development.

Histologic evaluation of BMEL regions in the subchondral trabecular compartment has 2 produced evidence of abnormalities in marrow constituents, in particular adipocyte necrosis and bone marrow fibrosis [1,8]. Changes in the trabecular compartment have been identified in cases of knee OA, including increased bone volume fraction, bone tissue necrosis, increased remodeling, and woven bone formation. Initial evidence has also shown that trabecular morphology and tissue mineral density is altered overall in OA joints [9]. Further, trabecular morphology appears to be altered focally within BMEL regions in comparison to regions outside BMEL [8]. Taken together, this evidence strongly suggests a closely coordinated interplay among bone, marrow, and cartilage changes in knee OA.

The long-term goal of this work is to understand the biological and mechanical pathways linking cartilage, bone, and marrow changes in the progression of OA. The aim of the present study was to evaluate the structure and composition of trabecular bone within BMEL regions associated with knee OA. We hypothesize that BMEL regions are foci of altered bone structure and composition, spatially associated with cartilage degradation. To address

this hypothesis, local spatial relationships between cartilage matrix composition and bone structure and composition were determined. Micro-computed tomography (μCT) and high-resolution peripheral quantitative computed tomography (HR-pQCT) – powerful tools for the quantification of density and microstructure of trabecular bone – were used to perform this work. Fourier transform infrared (FTIR) spectroscopy was used to quantify complementary indices of bone tissue composition, in particular metrics of mineral and collagen maturity. MR imaging was used to quantify metrics of cartilage composition. This work is novel in applying multi-modal advanced structural and compositional imaging techniques to the evaluation of BMEL.

Materials and Methods

Donor population

Twelve subjects (10 female, 2 male, mean age 70.6±10.4 yrs) with clinically diagnosed knee OA, who were scheduled for total knee arthroplasty (TKA), were recruited for this study. Patient recruitment occurred through referral from orthopaedic surgeons at the UCSF orthopaedic clinic. The UCSF Committee on Human Research approved the study protocol. Informed consent was obtained from each study participant prior to enrollment.

Specimen Collection and Processing

An overview of the specimen collection and processing sequence is presented in Figure 1. Tibial plateau specimens (n = 18, from 10 donors) were collected during TKA surgery. Each plateau was removed as a single piece with a reciprocating saw. The specimen was photographed to document orientation and condition, and then immediately transferred to the laboratory where a number of physical registration guides were affixed to the specimen. First, the distal face of the specimen was marked with a perpendicular set of shallow notches, to serve as a location reference for μCT imaging. A plastic grid was then affixed to the distal face, aligned with the notches, to serve as a location reference for MR and HR-pQCT imaging. The specimen with 1 attached plastic grid was then placed into a plastic container and immersed in lactated Ringer's 2 solution in preparation for MR scanning. Following MR scanning, the lactated Ringer's solution was drained and HR-pQCT scanning was performed.

After HR-pQCT imaging, the specimen was prepared for μCT imaging, FTIR spectroscopy, and histology. Two adjacent 3 mm-thick sagittal slices containing BMEL were identified based on the MR images; the medial slice was selected for μCT imaging and FTIR analysis, the lateral slice for histological processing. The slices were cut from the specimen using a precision sectioning saw (Buehler Ltd., Lake Bluff, IL), which was used to properly position the blade with respect to the guide notches.

MR Imaging

Specimens were scanned using a 3T MR scanner (Signa HDx, GE Healthcare, Milwaukee, WI, USA) with an eight-channel phased array transmit/receive knee coil (Invivo, Orlando, FL, USA). The MRI protocol included four sequences:

1. Sagittal T2-weighted fat-saturated fast spin-echo (FSE) images (TR/TE=4300/51ms, field of view [FOV] = 8mm, matrix = 512 * 256, slice thickness = 1 mm) for identifying BMEL.
2. Sagittal 3D fat suppressed high-resolution spoiled gradient-echo (SPGR) images (TR/TE = 15/6.7 ms, flip angle = 12, FOV = 8 cm, matrix = 512 × 512, slice thickness = 1 mm) for 9 cartilage segmentation.

3. A sagittal 3D T1ρ quantification sequence (FOV = 8 cm, matrix = 256 × 128, slice thickness = 2 mm, time of spin-lock = 0/10/40/80 ms, frequency of spin-lock = 500 Hz).
4. A sagittal 3D T2 quantification sequence (preparation TE = 3/14/25/46 ms, other parameters same as T1ρ).

MR Analysis – BMEL

BMEL were identified on the T2-weighted FSE images as focal subchondral high signal intensity areas. Subchondral cysts presenting as elliptical areas of hyperintense signal with well-defined borders were excluded, since cysts do not provide bone for morphological or densitometric analysis. A 3D contour containing each BMEL volume of interest (VOI) was generated semi-automatically using in-house developed software [7]. Each BMEL VOI was verified by a trained radiologist. A second contour encompassing only normal T2 signal was created for comparison within the same sagittal slice as the BMEL VOI (2 cm distance from BMEL perimeter, 3 mm diameter). Each non-BMEL VOI was placed at the same distance from the articular surface as its BMEL pair to minimize location bias. Anterior - posterior placement of the non-BMEL VOI was investigated in a sensitivity analysis and found to have no influence on structural parameters. Signal intensity within each BMEL and non-BMEL VOI was calculated using code written in IDL (Boulder, CO, USA).

Pre-operative MR images were not available for all donors in this study. However, a separate technique validation study of pre-operative and post-operative MR images using 10 knees confirmed that BMEL regions identified on ex vivo specimen MR scans are also present prior to surgical excision. To further preclude the possibility of identifying surgical trauma as BMEL, regions adjacent to the resection surface were excluded from consideration in this study.

MR Analysis – Cartilage

The $T_{1\rho}$ and T2 maps were reconstructed using in-house developed software written in C by fitting the $T_{1\rho}$-weighted and T2-weighted images pixel-by-pixel to the equation $S(TSL) \propto S_0*\exp(-TSL/T_{1\rho})$ and $S(TE) \propto S_0*\exp(-TE/T2)$, respectively. Cartilage was segmented semi-automatically in sagittal SPGR images using in-house developed MATLAB code based on edge detection and Bezier splines [10]. Three-dimensional cartilage contours were generated and overlaid onto FSE images. Regions of cartilage overlying BMEL and regions of surrounding 1 cartilage were defined manually (Fig. 1). The defined ROIs were then overlaid onto the reconstructed $T_{1\rho}$ and T2 maps. Mean, median and standard deviation (SD) of $T_{1\rho}$ and T2 values were calculated for each region.

HR-pQCT Imaging

Following MRI, if BMEL presented, specimens were scanned using a clinical HR-pQCT system (XtremeCT, Scanco Medical AG, Brüttisellen, Switzerland). For tomography, 1000 projections were acquired over 180 degrees with a 200 ms integration time at each angular position, with 60 kVp source potential and 900 μA current. The 12.6 cm field of view (FOV) was reconstructed across a 3072 × 3072 matrix using a modified Feldkamp algorithm, yielding isotropic 41 μm voxels. The reconstructed linear attenuation values were converted to hydroxyapatite (HA) mineral density values based on a separate scan of a density calibration phantom.

HR-pQCT Analysis

To locate BMEL and non-BMEL VOIs on the HR-pQCT images, MR-derived contours were overlaid onto the HR-pQCT data (Fig. 2). This was achieved by spatially registering

the MR images to HR-pQCT images using a 3D rigid registration algorithm based on normalized mutual information [11,12].

HR-pQCT image processing was performed in Image Processing Language (IPL, Scanco Medical AG). Reconstructed images were binarized to distinguish bone from background using an adaptive iterative threshold selection algorithm. Structural parameters were then calculated from the binarized volumes using direct three-dimensional methods [13]. BV/TV was measured by direct voxel counting of bone and background phases. Trabecular thickness (Tb.Th), separation (Tb.Sp), and number (Tb.N) were calculated using a skeletonization routine and a model-independent three-dimensional sphere filling technique [14,15,16]. Standard deviation of 1/Tb.N (Tb.1/N SD) was calculated as a measure of structural heterogeneity. Volumetric bone mineral density (vBMD) was calculated by taking the mean HA density for all voxels within each VOI.

μCT Imaging

A subset of 10 specimens from 6 donors was evaluated by μCT. Imaging was performed on a benchtop μCT scanner (μCT 40, Scanco AG) at a voxel size of 8 μm (isotropic) with a source potential of 70 kVp and current of 114 μA. Each scan consisted of 2000 projections over 360 degrees with each projection sampled for 250 ms. To minimize the influence of specimen volume fraction on reconstructed linear attenuation values, a scanner-specific beam hardening correction based on a 1200 mg HA/cm^3 wedge phantom was applied [17]. As for the HR-pQCT data, attenuation values of the reconstructed voxels were converted to HA concentration using a linear regression derived by imaging a calibration phantom.

For each specimen slice scanned by μCT, two regions were imaged; one covering the BMEL VOI identified on the T2-weighted FSE MR images, and the second covering the non-BMEL VOI. BMEL and non-BMEL VOI locations were identified with respect to the guide notches placed on the distal face of the specimen prior to imaging, which were visible on the μCT scout view during scan prescription.

μCT Analysis

Image processing was performed in IPL. Circular contours (3 mm diameter), placed within the BMEL and non-BMEL VOIs, were used to define regions for analysis in the μCT images (Fig. 2). Reconstructed images were binarized using an adaptive iterative threshold selection algorithm. Structural parameters were then calculated from the binarized volumes using direct three-dimensional methods as detailed above. In addition, structure model index (SMI), a measure of surface convexity, was calculated from a triangulated surface representation of the binary data [18]. Densitometric parameters vBMD and tissue mineral density (TMD) were calculated within each μCT analysis region. Two voxels were peeled from trabecular surfaces prior to calculating densitometric parameters to minimize partial volume effects.

FTIR Spectroscopy

Marrow was cleared from each slice by sonication and low-pressure water jet. The BMEL and non-BMEL regions analyzed by HR-pQCT and μCT were located, using the guide notches, and excised using a 3 mm diameter biopsy punch. Each FTIR sample was then desiccated through an ethanol series. For each sample, a homogenized powder mixture was created of 1% bone by weight in potassium bromide (KBr; Thermo Electron Corporation). Spectroscopy was performed on a benchtop interferometer system (Nexus 870, Thermo Electron Corporation). Spectra were acquired using 256 scans at a spectral resolution of 4 cm^{-1}. A background scan was recorded immediately following each sample scan to facilitate background correction.

FTIR Analysis

Following acquisition, the spectra were transferred to chemical imaging software (Isys, Spectral Dimensions, Inc.) for analysis. Spectra were baseline adjusted and the integrated areas of the amide I (1595-1720 cm^{-1}), $\nu1$ $\nu3$ phosphate (PO_4, 895-1215 cm^{-1}), and carbonate (CO_3^{2-}, 840-890 cm^{-1}) bands were calculated. Mineral-to-matrix (PO_4/amide I), carbonate-to-phosphate 2 (CO_3^{2-}/PO_4), and carbonate-to-matrix (CO_3^{2-}/amide I) ratios were calculated from integrated areas of the respective peaks. Additionally, peak heights were measured at specific wavenumbers: 1020 cm^{-1}, 1030 cm^{-1}, 1660 cm^{-1}, and 1690 cm^{-1}. From these, the following absorbance ratios were calculated to determine additional spectroscopic parameters. The ratio of 1030 cm^{-1} to 1020 cm^{-1} represents the ratio of stoichiometric apatite to non-stoichiometric apatite, a measure of crystallinity. The ratio of 1660 cm^{-1} to 1690 cm^{-1} represents collagen maturity.

Histological Analysis

The sagittal slice reserved for histology was fixed in 10% formalin and shipped to AML Laboratories (AML Laboratories, Inc, Baltimore, MD) for paraffin embedding, sectioning, and hematoxylin and eosin (H&E) staining.

Statistical Analysis

Means and standard deviations were calculated for all indices. Normality of distribution was confirmed for all data within the BMEL and non-BMEL regions, while Shapiro-Wilk W tests revealed that $T_{1\rho}$ and T2 values were not normally distributed. In the case where a tibial plateau was taken from each knee of a donor undergoing bilateral TKA, within-group effects were accounted for by the use of an ANOVA utilizing a mixed-effects model with repeated measures for differences between BMEL and non-BMEL regions, and by a Friedman rank sum test (a non-parametric version of ANOVA using a mixed-effects model) for differences between overlying and surrounding cartilage. Statistical analyses were performed in JMP (Version 7.0, SAS Institute Inc., Cary, NC) and R (v.2.13.0, http://www.r-project.org/foundation/).

Results

Of the 18 plateau specimens collected during TKA surgery, 16 were found to contain BMEL upon MR examination. Among the 16 remaining specimens, 11 had little or no cartilage overlying the BMEL region, leaving 5 specimens from 4 donors in which $T_{1\rho}$ and T2 quantification was possible. In these specimens, $T_{1\rho}$ values were elevated in cartilage overlying BMEL as compared to the surrounding cartilage (overlying: $T_{1\rho}$ 56.8±7.6 ms surrounding: 47.1±11.2 ms, $p = 0.046$; Fig. 3). T2 values followed the same trend but did not reach significance (one data point was excluded due to significant artifact in the image).

Analysis of μCT images (n = 10 images from 6 donors) yielded significant differences in structural and densitometric parameters between matched BMEL and non-BMEL regions (Table 1). Bone within BMEL regions had higher vBMD as compared to non-BMEL regions within the same tibial plateau (47% higher, $p = 0.016$). Volume fraction data also reflected elevated bone quantity within BMEL regions (62%, $p = 0.009$). Trabecular thickness was increased within BMEL regions (31%, $p = 0.003$) as was Tb.N (28%, $p = 0.027$), while Tb.Sp was decreased compared to non-BMEL regions (−21%, $p = 0.012$). Trabeculae were found to be more plate-like within BMEL regions, as indicated by a lower SMI value ($p = 0.051$). Bone structure within BMEL regions was found to be more homogeneous, as indicated by lower Tb.1/N SD values (−18%, $p = 0.018$). No difference was detected in μCT-based tissue mineral density (TMD) values ($p > 0.05$). Analysis of HR-pQCT data (n = 11 samples from 7 donors), which encompassed a larger, more inclusive

BMEL VOI, confirmed significant elevation of vBMD (88%, p = 0.002), BV/TV (23%, p = 0.026), and Tb.Th (21%, p < 0.001), and significant decrease of Tb.1/N SD (−33%, p = 0.025) within BMEL regions. HR-pQCT analysis did not find significant differences between BMEL and non-BMEL bone in the remaining structural measures.

FTIR analysis performed on n = 16 samples from 10 donors found significantly decreased mineral-to-matrix ratio in BMEL bone (−11%, p < 0.001; Fig.4). Mineral-to-matrix ratio was also lower in the BMEL tissue (−12%, p = 0.008) within the subset of specimens (n=10 samples from 6 donors) scanned by μCT. Carbonate-to-matrix ratio was lower in BMEL bone (−14%, p < 0.001). No differences were found in carbonate-to-phosphate ratio, crystallinity or collagen maturity.

Histological evaluation of BMEL regions revealed infiltration of marrow space by a fibrous collagen network (Fig. 5). Widespread evidence of woven bone and reversal lines indicated high turnover and active bone formation. These features were not evident in regions outside BMEL. BMEL bone appeared viable, with osteocyte nuclei evident throughout each slide. No microdamage was evident in these histological preparations. The histological appearance of cartilage overlying BMEL regions confirmed an advance stage of degradation, with fibrillation and erosion as well as increased vascularity superior to the tidemark.

Discussion

This study examined structure and composition of subchondral trabecular bone within BMEL in subjects with knee OA. Trabecular bone within BMEL was higher in volume fraction, with more and thicker trabeculae that were more plate-like in structure compared to unaffected regions of the tibial plateau. Trabecular tissue composition was also abnormal within the BMEL region, with decreased phosphate and carbonate content compared to tissue outside the lesion. Extensive marrow changes were present, including infiltration by a fibrous collagen network and evidence of increased remodeling activity. Moreover, MR cartilage analysis confirmed that these structural and compositional changes in bone and marrow were specifically localized to regions underlying cartilage degradation. Therefore these results support the paradigm of focal, site-specific interactions among bone, marrow, and cartilage in the progression of knee OA.

A strength of this study is the use of multiple imaging modalities to investigate the relationships between bone, cartilage, and marrow features at the macroscopic and tissue level in osteoarthritis. A second strength is the use of advanced image processing methodology, in particular the segmentation technique used to isolate BMEL regions on the T2-weighted fat-saturated FSE MR images and the registration process used to spatially align the BMEL contours onto the HR-pQCT and μCT images. These automated techniques reduce operator bias and ensure that solely BMEL tissue is included in each analysis. In addition, this study compared BMEL regions to non-BMEL regions in the same sagittal plane and therefore in the same tibial compartment (medial vs lateral). Spatial variation in bone morphology is known to exist in the osteaoarthritic tibial plateau [19], therefore a comparison within the same sagittal plane avoids bias due to extant variation between compartments. The application of FTIR spectroscopy to the analysis of BMEL tissue is novel. Finally, this study extends previous work by simultaneously quantifying cartilage degradation at the articular surface overlying the BMEL region, providing a comprehensive analysis of pathology localization in the OA knee.

Our findings are in agreement with previously published work indicating increased bone quantity and altered morphology subjacent to osteoarthritic joint surfaces. In the first μCT study to compare BMEL-affected areas to other areas within the same osteoarthritic tibial

plateau, Hunter et al found increased BV/TV and Tb.Th and more plate-like structure near zones of BMEL [8]. In their analysis, no alterations in BMEL Tb.N or Tb.Sp were detected, whereas our data show a 28% increase in Tb.N and 21% decrease in Tb.Sp within the BMEL regions. These morphological changes are consistent with sclerotic trabecular architectural pathology.

Previously published data have established the phenomenon of hypomineralized subchondral trabecular bone in OA. The literature to date has described mineral density and mineral-to-collagen ratio obtained through ash and hydroxyproline measurements [20,21,22,23]; these values were reported to be reduced in OA samples. The results of this study reveal that within subchondral trabecular bone the BMEL region, specifically, is a focal zone of hypomineralization. The FTIR spectroscopy measure mineral-to-matrix ratio increases as both primary and secondary mineralization progress and, therefore, is positively associated with tissue age [24,25]. The decreased mineral-to-matrix and carbonate-to-matrix values found within BMEL regions indicate the presence of an imbalance towards low mineralization. Metrics of mineral stoichiometry and collagen maturity, however, remained unchanged within BMEL tissue. In contrast to the FTIR results, μCT-based TMD quantification did not detect a significant difference between BMEL and non-BMEL tissue mineralization. The apparent inconsistency between techniques is likely driven by a number of technical considerations, including differences in the physical phenomena on which the two techniques are based, HA components detected, image analysis and sensitivity. This result underscores the complementary nature of FTIR and μCT techniques and the importance of multi-modality evaluation of bone quality.

Reports of bone turnover imbalances in OA [26,27] provide a likely mechanism for the accumulation of tissue with low mineralization. Increased collagen synthesis in the subchondral bone of osteoarthritic femoral heads, determined by C-terminal propeptide content, has been described in the literature [23]. Increased levels of bone resorption markers have been reported in subjects with OA compared to controls [28,29]. Analyses of the Boston Osteoarthritis of the Knee Study and the Framingham Osteoarthritis Study revealed an association between the presence of BMEL and increased type I collagen N-telopeptide (NTx), suggesting that turnover imbalance is extreme in OA subjects exhibiting BMEL [30]. Increased bone turnover within BMEL is supported by our histological analysis as well as data published by other groups showing increased osteoid volume within BMEL [31,32].

The morphologic features of BMEL reported here are consistent with enhanced mechanical properties; however, BMEL tissue mineralization is lower than neighboring unaffected bone. Importantly, FTIR measures of tissue mineralization are correlated with mechanical integrity of the tissue. Studies of human tissue and animal models demonstrated positive correlations between mineral-to-matrix ratio and tissue stiffness and hardness [24,33,34]. Mineral-to-matrix ratio explains 50–60% of the variation in both tissue modulus and hardness [25,35]. In our study, decreased mineral-to-matrix ratio within BMEL suggests reduced tissue stiffness. Accordingly, mechanical testing data describing apparent-level and tissue properties show decreased stiffness despite increased bone volume in osteoarthritic subchondral bone [36,37].

The source of the ill-defined hyperintensities seen on T2-weighted FSE images within regions of BMEL is not well understood. The fibrous collagen matrix visualized within the marrow space could explain this signal abnormality. The substitution of fibrous tissue for hydrophobic lipid in the marrow space would increase water content relative to healthy marrow, and thus increase signal on fluid-sensitive sequences. A positive association between BMEL signal intensity and lesion severity has been suggested [6]. This relationship

may be driven by progressive adipocyte necrosis and fibrous tissue infiltration as the lesion develops, which in turn increases relative fluid content and therefore signal intensity.

There are a number of limitations of this study that must be considered. First, BMEL regions were identified on post-operative MR scans rather than in vivo pre-operative scans. Damage during resection and handling could possibly lead to altered signal intensity on the post-operative MR image. The workflow of this study was designed specifically to minimize the chance of artifacts on the post-operative MR images, specifically by scanning specimens immediately after surgery and excluding regions adjacent to the resection surface from identification as BMEL. Second, data regarding pre-operative joint alignment were not available. This information would be instructive in interpreting the locations and interactions of cartilage, marrow, and bone abnormalities, particularly because malalignment may directly influence all three compartments. A third limitation is the small volume of trabecular bone analyzed via μCT. The size of the region was limited with the intention of analyzing identical volumes by μCT and FTIR. Because FTIR analysis requires a physical punch to be extracted, the 3 mm diameter maximized the available BMEL tissue. HR-pQCT analysis, however, was performed within the entire BMEL VOI and corroborated the results of μCT analysis for all comparisons that had high statistical significance in the μCT analysis ($p < 0.03$). For those μCT comparisons which achieved only moderate statistical significance ($p = 0.05$ to 0.03) the HR-pQCT analysis did not identify differences between BMEL and non-BMEL regions. This may be explained by the discrepancy in VOI location rather than volume; the μCT VOI was located at the center of the BMEL region, possibly the most severely altered location.

In summary, significant changes in trabecular structure, tissue composition, and marrow space constituents were found within BMEL regions in the subchondral compartment of human osteoarthritic tibias. Multi-modality imaging using quantitative MRI, high-resolution quantitative μCT and Fourier transform infrared (FTIR) spectroscopy are powerful tools in providing quantitative and comprehensive assessment of cartilage, bone, and marrow pathology in osteoarthritis.

Acknowledgments

The authors acknowledge the valuable assistance of J.B. Pialat, MD and Christoph Stehling, MD in reviewing MR images, Janet Goldenstein, PhD for consulting on image registration, and Andrew Burghardt for consulting on image analysis. This publication was supported by the UCSF Dept of Radiology and Biomedical Imaging Pilot Grant Program (GJK, XL), NIH K01 AR056734 (GJK), NIH K25 AR053633 and R21AR056773 (XL), and NIH RO1 AG17762 (SM). Funding sources had no involvement in the design or execution of the study, or in the decision to submit the manuscript for publication.

Funding: UCSF Department of Radiology and Biomedical Imaging Pilot, Grant Program (GJK, XL), NIH K01 AR056734 (GJK), NIH K25 AR053633 and R21AR056773 (XL), NIH RO1 AG17762 (SM)

References

1. Zanetti M, Bruder E, Romero J, Hodler J. Bone marrow edema pattern in osteoarthritic knees: correlation between MR imaging and histologic findings. Radiology. 2000; 215:835–840. [PubMed: 10831707]
2. Felson DT, Chaisson CE, Hill CL, Totterman SM, Gale ME, Skinner KM, et al. The association of bone marrow lesions with pain in knee osteoarthritis. Ann Intern Med. 2001; 134:541–549. [PubMed: 11281736]
3. Sowers MF, Hayes C, Jamadar D, Capul D, Lachance L, Jannausch M, et al. Magnetic resonance-detected subchondral bone marrow and cartilage defect characteristics associated with pain and X-ray-defined knee osteoarthritis. Osteoarthritis Cartilage. 2003; 11:387–393. [PubMed: 12801478]

4. Felson DT, McLaughlin S, Goggins J, LaValley MP, Gale ME, Totterman S, et al. Bone marrow edema and its relation to progression of knee osteoarthritis. Ann Intern Med. 2003; 139:330–336. [PubMed: 12965941]
5. Hunter DJ, Zhang Y, Niu J, Goggins J, Amin S, LaValley MP, et al. Increase in bone marrow lesions associated with cartilage loss: a longitudinal magnetic resonance imaging study of knee osteoarthritis. Arthritis Rheum. 2006; 54:1529–1535. [PubMed: 16646037]
6. Zhao J, Li X, Bolbos RI, Link TM, Majumdar S. Longitudinal assessment of bone marrow edema-like lesions and cartilage degeneration in osteoarthritis using 3 T MR T1rho quantification. Skeletal Radiol. 2010; 39:523–531. [PubMed: 20195865]
7. Li X, Ma BC, Bolbos RI, Stahl R, Lozano J, Zuo J, et al. Quantitative assessment of bone marrow edema-like lesion and overlying cartilage in knees with osteoarthritis and anterior cruciate ligament tear using MR imaging and spectroscopic imaging at 3 Tesla. J Magn Reson Imaging. 2008; 28:453–461. [PubMed: 18666183]
8. Hunter DJ, Gerstenfeld L, Bishop G, Davis AD, Mason ZD, Einhorn TA, et al. Bone marrow lesions from osteoarthritis knees are characterized by sclerotic bone that is less well mineralized. Arthritis Res Ther. 2009; 11:R11. [PubMed: 19171047]
9. Ding M, Odgaard A, Hvid I. Changes in the three-dimensional microstructure of human tibial cancellous bone in early osteoarthritis. J Bone Joint Surg Br. 2003; 85:906–912. [PubMed: 12931817]
10. Carballido-Gamio J, Bauer JS, Stahl R, Lee KY, Krause S, Link TM, et al. Inter-subject comparison of MRI knee cartilage thickness. Med Image Anal. 2008; 12:120–135. [PubMed: 17923429]
11. Studholme C, Hill DLG, Hawkes DJ. An overlap invariant entropy measure of 3D medical image alignment. Pattern Recognition. 1999; 32:71–86.
12. Goldenstein J, Kazakia G, Majumdar S. In vivo evaluation of the presence of bone marrow in cortical porosity in postmenopausal osteopenic women. Ann Biomed Eng. 2010; 38:235–246. [PubMed: 19953321]
13. Burghardt AJ, Kazakia GJ, Majumdar S. A local adaptive threshold strategy for high resolution peripheral quantitative computed tomography of trabecular bone. Ann Biomed Eng. 2007; 35:1678–1686. [PubMed: 17602299]
14. Hildebrand T, Rüegsegger P. A new method for the model-independent assessment of thickness in three-dimensional images. Journal of Microscopy. 1997; 185:67–75.
15. Laib A, Hildebrand T, Häuselmann HJ, Rüegsegger P. Ridge number density: a new parameter for in vivo bone structure analysis. Bone. 1997; 21:541–546. [PubMed: 9430245]
16. Muller R, Hildebrand T, Ruegsegger P. Non-invasive bone biopsy: a new method to analyse and display the three-dimensional structure of trabecular bone. Phys Med Biol. 1994; 39:145–164. [PubMed: 7651993]
17. Kazakia GJ, Burghardt AJ, Cheung S, Majumdar S. Assessment of bone tissue mineralization by conventional x-ray microcomputed tomography: comparison with synchrotron radiation microcomputed tomography and ash measurements. Med Phys. 2008; 35:3170–3179. [PubMed: 18697542]
18. Hildebrand T, Ruegsegger P. Quantification of Bone Microarchitecture with the Structure Model Index. Comput Methods Biomech Biomed Engin. 1997; 1:15–23. [PubMed: 11264794]
19. Patel V, Issever AS, Burghardt A, Laib A, Ries M, Majumdar S. MicroCT evaluation of normal and osteoarthritic bone structure in human knee specimens. J Orthop Res. 2003; 21:6–13. [PubMed: 12507574]
20. Ding M, Danielsen CC, Hvid I. Age-related three-dimensional microarchitectural adaptations of subchondral bone tissues in guinea pig primary osteoarthrosis. Calcif Tissue Int. 2006; 78:113–122. [PubMed: 16397735]
21. Karvonen RL, Miller PR, Nelson DA, Granda JL, Fernandez-Madrid F. Periarticular osteoporosis in osteoarthritis of the knee. J Rheumatol. 1998; 25:2187–2194. [PubMed: 9818663]
22. Li B, Aspden RM. Composition and mechanical properties of cancellous bone from the femoral head of patients with osteoporosis or osteoarthritis. Journal of Bone and Mineral Research. 1997; 12:641–651. [PubMed: 9101376]

23. Mansell JP, Bailey AJ. Abnormal cancellous bone collagen metabolism in osteoarthritis. J Clin Invest. 1998; 101:1596–1603. [PubMed: 9541489]
24. Gourion-Arsiquaud S, Faibish D, Myers E, Spevak L, Compston J, Hodsman A, et al. Use of FTIR spectroscopic imaging to identify parameters associated with fragility fracture. J Bone Miner Res. 2009; 24:1565–1571. [PubMed: 19419303]
25. Miller LM, Little W, Schirmer A, Sheik F, Busa B, Judex S. Accretion of bone quantity and quality in the developing mouse skeleton. J Bone Miner Res. 2007; 22:1037–1045. [PubMed: 17402847]
26. Hopwood B, Tsykin A, Findlay DM, Fazzalari NL. Microarray gene expression profiling of osteoarthritic bone suggests altered bone remodelling, WNT and transforming growth factor-beta/bone morphogenic protein signalling. Arthritis Res Ther. 2007; 9:R100. [PubMed: 17900349]
27. Hunter DJ, Spector TD. The role of bone metabolism in osteoarthritis. Curr Rheumatol Rep. 2003; 5:15–19. [PubMed: 12590880]
28. Bettica P, Cline G, Hart DJ, Meyer J, Spector TD. Evidence for increased bone resorption in patients with progressive knee osteoarthritis: longitudinal results from the Chingford study. Arthritis Rheum. 2002; 46:3178–3184. [PubMed: 12483721]
29. Hunter DJ, Hart D, Snieder H, Bettica P, Swaminathan R, Spector TD. Evidence of altered bone turnover, vitamin D and calcium regulation with knee osteoarthritis in female twins. Rheumatology (Oxford). 2003; 42:1311–1316. [PubMed: 12867590]
30. Hunter DJ, Lavalley M, Li J, Bauer DC, Nevitt M, DeGroot J, et al. Biochemical markers of bone turnover and their association with bone marrow lesions. Arthritis Res Ther. 2008; 10:R102. [PubMed: 18759975]
31. Plenk H Jr. Hofmann S, Eschberger J, Gstettner M, Kramer J, Schneider W, et al. Histomorphology and bone morphometry of the bone marrow edema syndrome of the hip. Clin Orthop Relat Res. 1997:73–84. [PubMed: 9005898]
32. Thiryayi WA, Thiryayi SA, Freemont AJ. Histopathological perspective on bone marrow oedema, reactive bone change and haemorrhage. Eur J Radiol. 2008; 67:62–67. [PubMed: 18337044]
33. Camacho NP, Rimnac CM, Meyer RA Jr. Doty S, Boskey AL. Effect of abnormal mineralization on the mechanical behavior of X-linked hypophosphatemic mice femora. 0 Bone. 1995; 17:271–278. [PubMed: 8541141]
34. Courtland HW, Nasser P, Goldstone AB, Spevak L, Boskey AL, Jepsen KJ. Fourier transform infrared imaging microspectroscopy and tissue-level mechanical testing reveal intraspecies variation in mouse bone mineral and matrix composition. Calcif Tissue Int. 2008; 83:342–353. [PubMed: 18855037]
35. Donnelly E, Chen DX, Boskey AL, Baker SP, van der Meulen MC. Contribution of mineral to bone structural behavior and tissue mechanical properties. Calcif Tissue Int. 2010; 87:450–460. [PubMed: 20730582]
36. Brown SJ, Pollintine P, Powell DE, Davie MW, Sharp CA. Regional differences in mechanical and material properties of femoral head cancellous bone in health and osteoarthritis. Calcif Tissue Int. 2002; 71:227–234. [PubMed: 12170373]
37. Day JS, Ding M, van der, Linden JC, Hvid I, Sumner DR, Weinans H. A decreased subchondral trabecular bone tissue elastic modulus is associated with pre-arthritic cartilage damage. J Orthop Res. 2001; 19:914–918. [PubMed: 11562141]

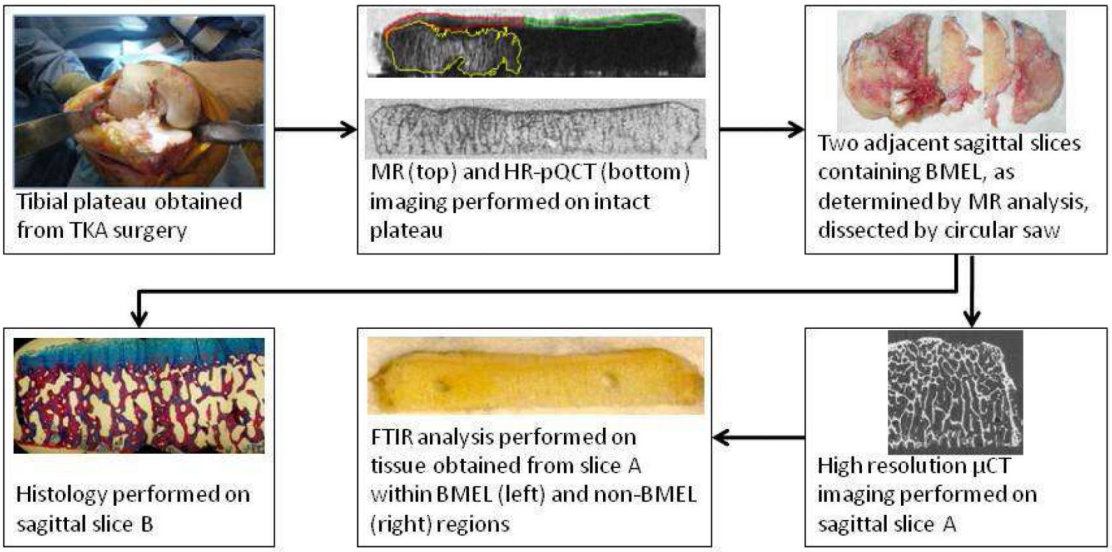

Figure 1.

Schematic of study workflow. The tibial plateau is obtained during surgery and scanned via MR and HR-pQCT. A contour delineating the BMEL region is defined on T2-weighted FSE images and transformed to the HR-pQCT coordinate system following spatial registration of the two data sets. Cartilage overlying BMEL (red) is differentiated from surrounding cartilage (green) and overlaid onto the reconstructed $T_{1\rho}$ and T_2 maps for cartilage parameter calculation. Adjacent slices containing BMEL are dissected from the specimen and processed for μCT imaging and FTIR spectroscopy (slice A) and histology (slice B).

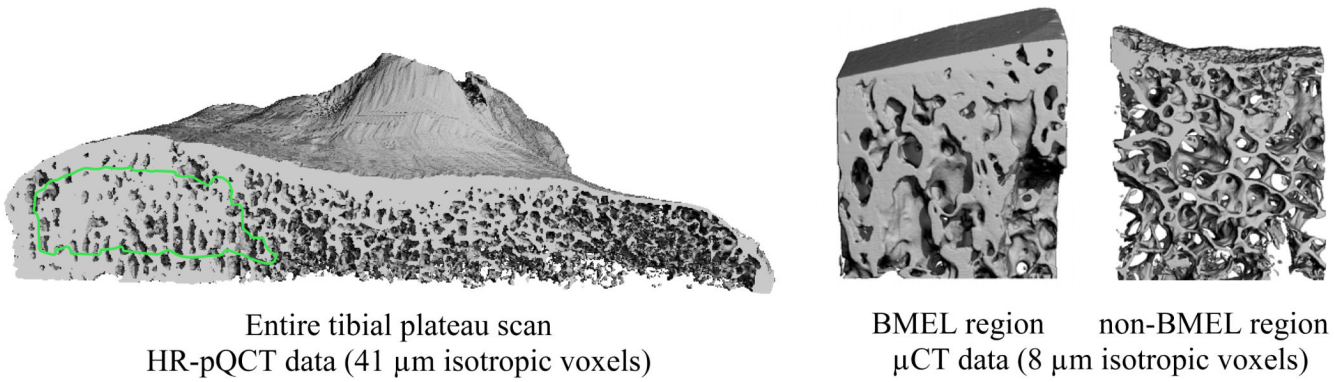

Figure 2.
Representative renderings of HR-pQCT and μCT data. Left: Sagittal cut-away view of a HR-pQCT scan of the entire tibial plateau, with BMEL analysis contour overlaid. Right: μCT scans of a BMEL and a non-BMEL region, with analysis region overlaid.

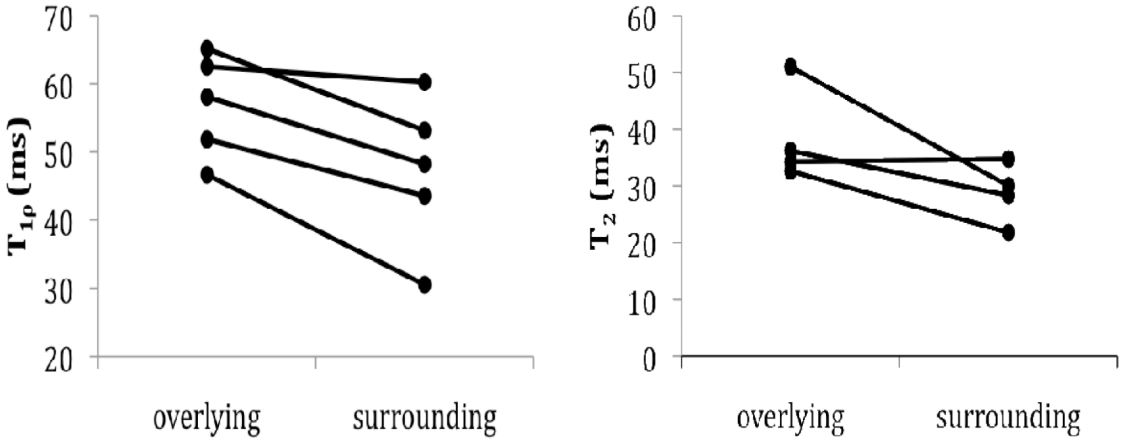

Figure 3.
$T_{1\rho}$ and T_2 values in cartilage overlying BMEL regions compared to those in surrounding cartilage. $T_{1\rho}$ values (left, n = 5 from 4 donors) were significantly higher (p = 0.046) in the cartilage overlying the lesion. T_2 values (left, n = 4 from 3 donors) followed the same trend but did not reach significance.

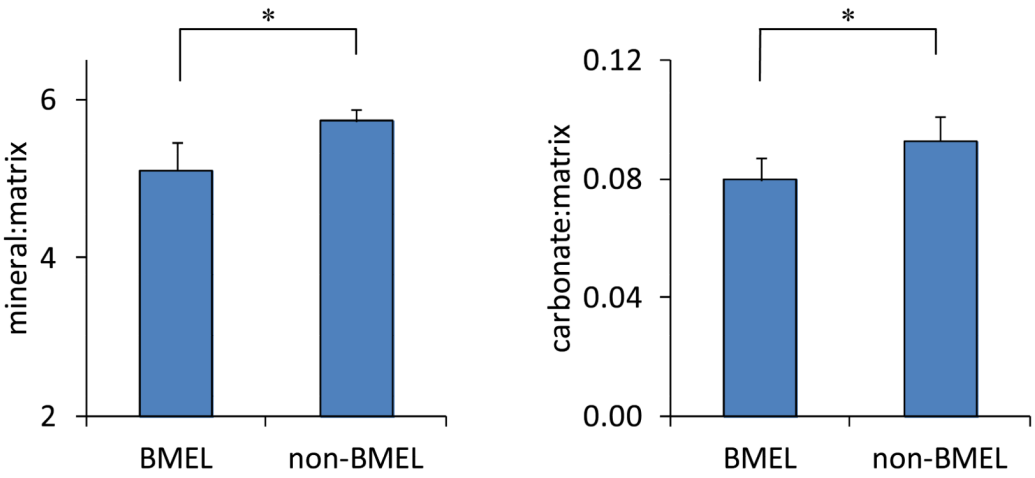

Figure 4.
FTIR parameter values within BMEL regions compared to those in non-BMEL bone (n = 16 from 10 donors). Mineral-to-matrix ratio (left, $p < 0.001$) and carbonate-to-matrix ratio (right, $p = 0.008$) were reduced within BMEL tissue. Error bars indicate 95% confidence intervals.

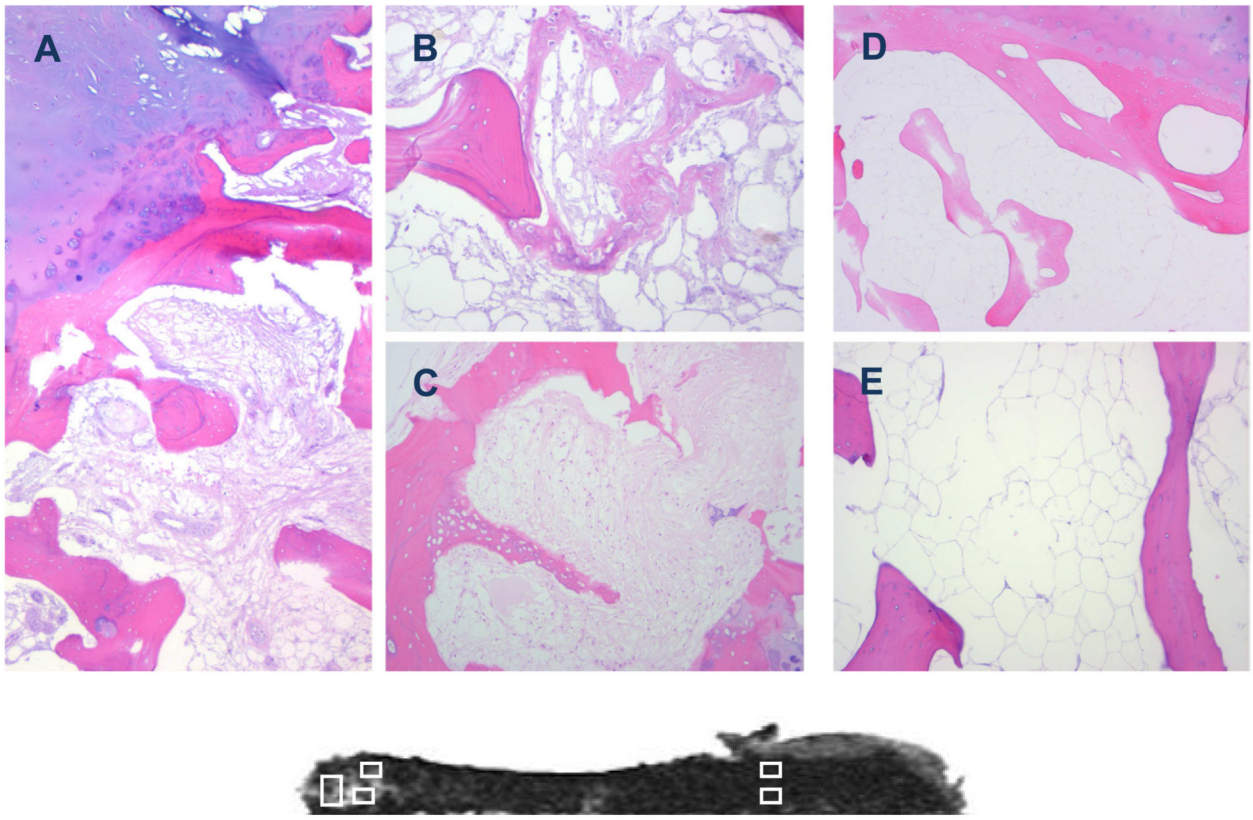

Figure 5.
Histological sections (H&E stained) taken from regions of the tibial plateau with evidence of BMEL (A, B, C) and without BMEL (D, E). The corresponding T2-weighted fat-saturated FSE image is shown below for reference. BMEL regions display mixed pathology including infiltration of marrow space by fibrous collagen network (A, B, C), bone remodeling (A) and formation (B, C). Fibrillation of overlying cartilage can also be seen (A). Tissues taken from uninvolved regions of the tibial plateau show none of these features, but rather confirm quiescent bone with adipocyte-filled marrow space (D, E).

Table 1

Structural and densitometric parameters quantified by μCT analysis (mean ± standard deviation) within bone marrow lesions (BMEL) and outside the lesions (non-BMEL).

μCT	BMEL	Non-BMEL	%diff	P*
BV/TV	0.33 ± 0.12	0.20 ± 0.05	62	0.009
Tb.Th (mm)	0.20 ± 0.04	0.16 ±0.02	31	0.003
Tb.Sp (mm)	0.51 ±0.15	0.65 ±0.08	−21	0.012
Tb.N (1/mm)	1.87 ±0.56	1.46 ±0.16	28	0.027
Tb 1/N SD (mm)	0.20 ±0.05	0.24 ±0.03	−18	0.018
SMI	0.48 ±0.59	0.93 ±0.36	−49	0.051
vBMD (mgHA/cm^3)	358 ± 121	243 ± 50	47	0.016
TMD (mqHA/cm^3)	870 ± 32	882 ± 37	−1	NS

* mixed-design ANOVA. n=10 samples from 6 donors